PERGAMON

International Journal of Heat and Mass Transfer 46 (2003) 443–455

International Journal of HEAT and MASS TRANSFER

www.elsevier.com/locate/ijhmt

Localized flow and heat transfer interactions in louvered-fin arrays

N.C. DeJong [a], A.M. Jacobi [b,*]

[a] Department of Mechanical and Aerospace Engineering, San José State University, One Washington Square, San José, CA 95192-0087, USA

[b] Department of Mechanical and Industrial Engineering, University of Illinois at Urbana–Champaign, 1206 W. Green Street, Urbana, IL 61801, USA

Received 24 August 1999; received in revised form 22 July 2002

Abstract

A detailed study of flow, heat transfer, and pressure drop for louvered fins is presented. Louver-by-louver mass transfer data are acquired for Reynolds numbers from 130 to 1400. Pressure-drop data are obtained using a low-speed wind tunnel and local flow structures are visualized using dye injection in a water tunnel. Particular attention is placed on the role of vortex shedding in heat transfer enhancement. In contrast to recent studies for similar offset-strip arrays, vortex shedding is found to have less impact in louvered-fin arrays. Several practical implications for heat exchanger design and analysis are discussed.

Keywords: Convective heat transfer; Heat exchangers

1. Introduction

In many compact heat exchanger applications, interrupted-fin surfaces are used to enhance the air-side heat transfer performance. Interrupted surfaces restart the thermal boundary layers and, since the average boundary-layer thickness is smaller for short plates than for long plates, the average heat transfer coefficient is higher for an interrupted surface than for a continuous surface. Furthermore, above some critical Reynolds number, interrupted surfaces can cause vortex shedding which may enhance heat transfer. One common interrupted-surface design is the louvered-fin surface (Fig. 1). Only in the last two decades has much research on contemporary louvered-fin designs been reported in the open literature. Much of the existing research has focused on full-scale testing [1–5] and the development of numerical simulations or semi-empirical models [6–11]. Although somewhat counter-intuitive, prior studies have firmly established that the flow through louver arrays is *duct-directed* at very low Reynolds numbers; that is, it passes through the ducts created by neighboring fins as shown in Fig. 1. At higher Reynolds numbers, the flow becomes more *louver-directed* and follows the louvers rather than remaining in the ducts [6,12,13]. In the technical literature related to louvered-fin performance, the degree to which the flow follows the louvers is called *flow efficiency* (see Fig. 2). Several studies have shown a dramatic reduction in heat transfer performance when the flow efficiency is low [1–3,14]. The overall, macroscopic flow and heat transfer behavior—the flow efficiency and its impact on heat transfer—are fairly well understood, and thorough reviews of the literature are available [14,15]. However, localized and transient flow features and their effect on heat transfer are not very well understood. There has been numerical progress (see reviews [16,17]), with very recent numerical work showing the importance of local and transient effects [18–20]. However, other than a recent study of the entry region

* Corresponding author. Tel.: +1-217-333-4108; fax: +1-217-244-6534.

E-mail addresses: ndejong@email.sjsu.edu (N.C. DeJong), a-jacobi@uiuc.edu (A.M. Jacobi).

0017-9310/03/$ - see front matter
PII: S0017-9310(02)00292-2

Nomenclature

A_f	naphthalene surface area on fin specimen
D_{na}	mass diffusivity of naphthalene in air
d_t	measured transverse distance traveled by a streakline (see Fig. 2)
d'_t	ideal transverse distance traveled for perfectly louver-directed flow (see Fig. 2)
Eu	Euler number (see Eq. (4))
F_p	fin pitch (see Fig. 1)
$\bar{h}$	average heat transfer coefficient
$\bar{h}_m$	average mass transfer coefficient (see Eq. (2))
k	thermal conductivity of air
L_g	louver gap (see Fig. 1)
L_p	louver pitch (see Fig. 1)
$\overline{Nu}$	average Nusselt number, $\bar{h}L_p/k$
Pr	Prandtl number, ν/α
Re	Reynolds number (see Eq. (1))
Sc	Schmidt number, ν/D_{na}
$\overline{Sh}$	average Sherwood number based on louver pitch (see Eq. (3))
U_c	average velocity immediately downstream from the leading edge of the inlet louvers

Greek symbols

α	thermal diffusivity of air
Δm	change mass due to sublimation
ΔP	pressure drop across louver array
Δt	specimen exposure period to sublimation
η	flow efficiency (see Eq. (6))
ν	kinematic viscosity
θ	louver angle
ρ	mass density of air
$\rho_{n,v}$	mass density of saturated naphthalene vapor
$\rho_{n,\infty}$	mass density of naphthalene in the free-stream

provided by Springer and Thole [21], and a much earlier study by Aoki et al. [22] giving experimental heat transfer data on a louver-by-louver basis, no experimental information on these effects is available. Springer and Thole [21] provide only velocity information, and Aoki et al. [22] limit their heat transfer study to $Re \leqslant 450$, where unsteadiness and vortex shedding are not manifest.

The goal of this paper is to present a more complete experimental description of flow and heat transfer in louvered-fin arrays, with a focus on the physics important to thermal–hydraulic performance. A better understanding of flow and heat transfer interactions is possible through complementary experiments that provide louver-by-louver convective data, overall heat transfer behavior, pressure drop, and detailed flow vi-

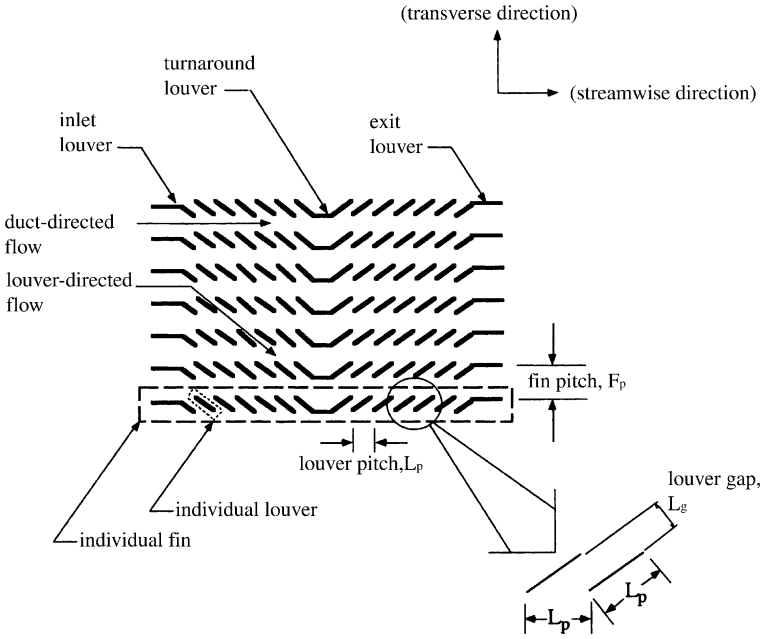

Fig. 1. Schematic of a louvered-fin array showing duct- and louver-directed flow.

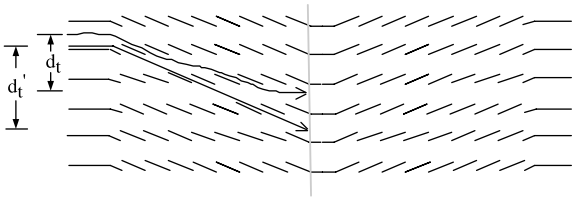

Fig. 2. Here flow efficiency is defined as $\eta = d_t/d_t'$ where d_t is the transverse distance traveled by the flow and d_t' is the transverse distance the flow would have traveled if it immediately became completely aligned with the louvers.

sualization. Attention will be focused on vortex shedding and its effects on heat transfer. Although vortex shedding has been noted to occur in louvered-fin arrays [13,23,24], [1] its influence on the thermal–hydraulic performance of these arrays has been largely ignored, and an assessment of its heat transfer and pressure-drop effects has not been previously reported for louvered-fin arrays. The reason for our interest in vortex shedding is that it has been shown to be very important to heat transfer enhancement in a closely related offset-strip array [26–29]. Understanding the impact of vortex shedding on louvered-fin performance could be important in developing improved designs.

2. Method

Exploiting the heat and mass transfer analogy, mass transfer experiments were conducted to measure louver-by-louver convective behavior. The naphthalene sublimation technique was used, and thorough reviews of this method and its application have appeared in the literature [30,31]. In addition to naphthalene sublimation and pressure-drop experiments performed in a low-speed wind tunnel, a complementary flow visualization study was conducted in a water tunnel. Further information on the apparatus, instrumentation, specimen preparation method, and experimental procedures used in this study can be found in [15] and [29].

2.1. Apparatus and instrumentation

The wind tunnel used in the mass transfer and pressure drop measurements provided an approach velocity that was flat to within approximately 2% with a turbulence intensity of about 0.5% [15]. The test section was constructed of clear acrylic and had movable side walls, creating a flow cross-section 7.1 cm high by 15.2–24.3 cm wide, depending on the location of the side walls. In this way, test arrays of different widths could be accommodated. The dimensions of the arrays tested are given in Table 1. The results of DeJong [15] showed flow in the center of the twelve- and fifteen-fin arrays to be periodic in the transverse direction, i.e., the wind tunnel walls had a negligible effect on flow in the center of a large array. The fin span (Fig. 1) was 7.06 cm, and the louver pitch was 1.19 cm for all samples. An array was placed in the test section, and platinum RTDs and static pressure taps were located upstream and downstream of the test array. Louvers in the center of the array were coated with naphthalene, and the rest of the array was constructed of dummy (uncoated) louvers. It was determined that when a proper driving potential was used in data interpretation, the mass transfer coefficients did not depend on whether dummy or naphthalene-coated louvers were used upstream of a given louver specimen. An identical finding was reported by DeJong et al. [32] for related offset-strip arrays. [2] Furthermore, DeJong [15] reported this finding for several three-fin louver arrays, and Aoki et al. [22] reported the same conclusion for a louvered-fin sample. At the Reynolds numbers of this study, the species (thermal) wakes have little or no effect on the mass (heat) transfer coefficients of downstream louvers. Thus, the presence or absence of naphthalene on upstream louvers has no discernible effect on convection downstream in the array (to within the 5% uncertainty of the measurements). The experiments reported here were sometimes conducted without a full array of naphthalene-coated louvers, and the results are expected to be independent of whether dummy louvers or coated louvers were used upstream of the test specimen. Naphthalene was only placed to cover the middle third of the specimen span, but the coating extended from the leading to the trailing edge on both sides of each specimen. The edges of the fins (across the $t = 1.2$ mm face) were treated so that no sublimation occurred from these faces. These precautions in specimen design

Table 1
Parameters of samples tested

θ (degrees)	F_p/L_p	Number of fins
18	1.09	12
28	1.09	12
22	1.2	15

[1] Antoniou et al. [25], also reported vortex shedding; however, their study used a seven-fin array, and the results of DeJong [15] and Springer and Thole [24] indicate that such a small array may not be representative of the periodic conditions of a large array.

[2] An offset-strip geometry consists of a staggered array of louvers at a zero attack angle to the approaching flow. This approach does not contradict the findings of Zhang and Tafti [19], in which the importance of the thermal wake is established. Thermal wake effects are experimental modeled as species-wake effects.

ensured that the wind tunnel wall effects and geometric distortion of the specimens were minimized. The maximum (spatially averaged) sublimation depth was always less than 5% of the louver thickness.

For the complementary flow visualization experiments, a water tunnel of a construction similar to the wind tunnel was used. The flow was visualized by injecting dye into it and recording the resulting images with standard photographic equipment. The same model fin arrays were used in both the wind tunnel and the water tunnel experiments.

2.2. Experimental procedure

For the mass transfer experiments, the naphthalene-coated test louvers were first weighed individually using an analytical balance. The specimens were then placed in the test array and exposed to a controlled air flow. Following exposure in the tunnel, the specimens were weighed again. During each run, upstream and downstream temperatures were sampled every 5 s and averaged over the period of the test. The core pressure drop, pressure drop across an ASME standard orifice plate (to determine flow rate), relative humidity, barometric pressure, and exposure time were also recorded.

Flow visualization was performed by injecting ink at various locations approximately 3 cm upstream of the inlet louver. Flow velocities were determined from the average transit time required for an ink flow marker to pass through a longer open section upstream of the array.

2.3. Data reduction and interpretation

The Reynolds number for flow through the test section was defined as

$$Re = U_c L_p / \nu \tag{1}$$

where U_c is the flow velocity at a cross-sectional plane just downstream from the leading edges of the inlet louvers. Davenport [1,2] found his data to be correlated better by louver pitch than by hydraulic diameter, and thus it has become conventional to base the Reynolds number for the louvered-fin geometry on louver pitch.

The average mass transfer coefficient was determined through

$$\bar{h}_m = \Delta m / (A_f(\rho_{n,v} - \rho_{n,\infty})\Delta t) \tag{2}$$

where Δm is the change in mass of the specimen, Δt is the exposure time, $\rho_{n,v}$ is the naphthalene vapor pressure at the fin surface, and $\rho_{n,\infty}$ is the local free-stream (or mixing-cup) concentration. The local value for $\rho_{n,\infty}$ was found by accounting for any mass transfer from upstream specimens (see DeJong [15] for further details).

The average Sherwood number was calculated using

$$\overline{Sh} = \bar{h}_m L_p / D_{na} \tag{3}$$

The core pressure drop, ΔP, was interpreted using the Euler number. Since the geometries studied have different hydraulic diameters but equivalent flow lengths, it is easier to understand the pressure-drop behavior using the Euler number rather than the friction factor.

$$Eu = 2\Delta P / (\rho U_c^2) \tag{4}$$

Heat transfer data can be inferred from the mass transfer data by employing the heat and mass analogy:

$$\overline{Nu} = \overline{Sh}(Pr/Sc)^{0.4} \tag{5}$$

For interrupted surfaces such as the louver array, taking the value of the exponent as 0.4 in the analogy is appropriate at intermediate values of Schmidt number [33].

Although alternate definitions have been proposed, for the purposes of this paper the flow efficiency of the louver array is defined as follows (refer to Fig. 2):

$$\eta = d_t / d_t' \tag{6}$$

2.4. Uncertainty

Uncertainties in the reduced data were estimated using standard methods [34]. The uncertainties in *Re* for the wind tunnel and water tunnel were less than 2% and 10%, respectively. The uncertainty in $\overline{Sh}$ was 5%. The uncertainty in ΔP decreased as the Reynolds number increased because the pressure measurement uncertainty was fixed. Therefore, uncertainties in ΔP ranged from approximately 50% at very low Reynolds numbers to 0.2% at high Reynolds numbers. Above a Reynolds number of 1000, the average uncertainty in ΔP was 1%, leading to an average uncertainty in *Eu* of about 4%. Based on the photographic and image-analysis resolution and repeated measurements at various locations throughout the array, η is estimated to have an uncertainty of less than 10%.

3. Results

3.1. Flow visualization and pressure-drop results

As discussed earlier, at very low Reynolds numbers flow through louvered-fin arrays can be characterized as *duct flow* whereas at higher Reynolds numbers it becomes a *louver-directed flow*. The flow follows the path of least resistance—the path corresponding to the lowest overall pressure drop. The total pressure drop is due to contributions from two mechanisms: friction drag and form drag. Bodoia and Osterle (see [35]) report that for a fixed average velocity, the pressure drop for developing

flow in a flat duct (friction drag) decreases as the duct diameter increases. So we expect friction drag to be lower in duct flow than in louver-directed flow for the usual case of $F_p > L_g$. The form drag for flow over a flat plate aligned with the flow is less than the form drag for flow over an inclined plate. So we expect form drag is lower for louver-directed flow (where the flow has a nearly zero angle of attack to the louvers) than for duct flow (where the flow has a non-zero degree angle of attack to the louvers). Therefore, with friction drag favoring duct flow and form drag favoring louver-direct flow, these two mechanisms compete to establish the flow efficiency. At low Reynolds numbers the first effect dominates, and the flow is largely duct-directed. However, as the Reynolds number increases, the friction drag increases at a slower rate than the form drag, and eventually louver-directed flow is favored.

Flow efficiency versus Reynolds number for three different arrays is provided in Fig. 3. Completely louver-directed flow has a flow efficiency of "1" whereas completely duct-directed flow has a flow efficiency of "0". Bellows [13] performed flow visualization for similar louver arrays and reported similar results. These new data and those of Bellows show a maximum flow efficiency of 0.77 for the geometry with $\theta = 28°$ and $F_p/L_p = 1.09$. For all the arrays, Fig. 3 shows that the flow efficiency asymptotically approaches its maximum value as the Reynolds number increases; i.e., above a certain Reynolds number the flow efficiency is approximately constant, its value depending on the array geometry.

Fig. 3 also shows that as the louver angle increases (from 18° to 28°) the flow becomes more louver-directed. Two mechanisms are at work here. First, as Fig. 4 shows in a somewhat exaggerated fashion, the duct diameter effectively decreases with an increase in louver angle. Thus, the friction drag for flow through the duct increases, and the path of least resistance passes through the louvers to a higher degree. Second, as the louver angle increases, there is a greater pressure-drop penalty due to form drag associated with duct-directed flow, and the path of least resistance becomes more and more louver-directed. Pressure drop and flow efficiency are intimately related. Fig. 5 shows that as the louver angle increases, the total pressure drop increases as well. While an increase in the louver angle will result in an increase in the pressure drop, an increase in F_p/L_p can offset this effect, as the *Eu* results for the geometry with $\theta = 22°$ and $F_p/L_p = 1.2$ indicate. Flow through a geometry with a larger louver angle becomes louver-directed at a lower Reynolds number. For the present case with $F_p/L_p = 1.09$, the flow efficiency for the geometry with $\theta = 18°$ approximately doubles from $Re = 134$ to 254. The flow efficiency for the geometry with $\theta = 28°$ shows a similar increase but from $Re = 79$ to 104. There are not enough

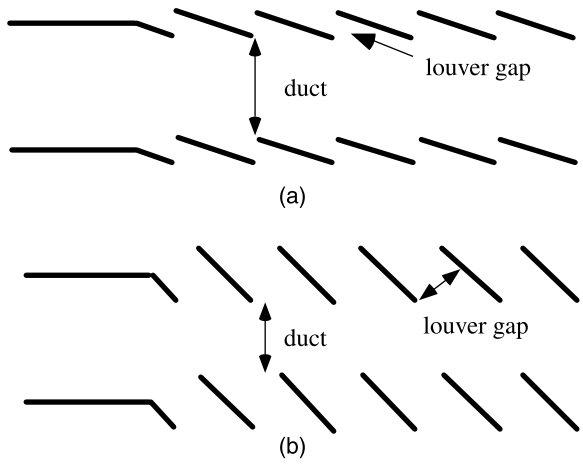

Fig. 4. Schematic showing how the duct width decreases and louver gap size increases when the louver angle increases.

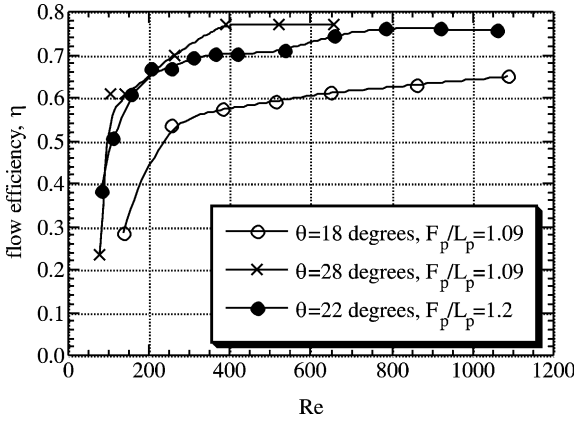

Fig. 3. Flow efficiency versus Reynolds number for three different arrays.

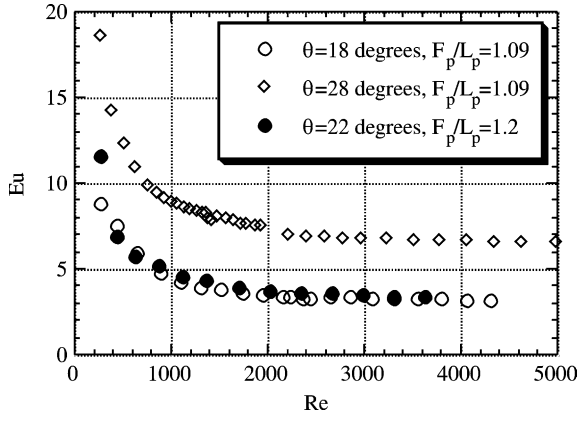

Fig. 5. Plot showing the effect of louver angle on pressure drop.

data presented here to clearly show the effect of fin- to louver-pitch ratio on flow efficiency, but Webb and Trauger [12] show that as this ratio increases, the flow efficiency decreases. The data in Fig. 6 confirm that as F_p/L_p decreases, the total pressure drop through the array increases. For a complete discussion of the causes of these changes in flow efficiency with geometry, see DeJong [15].

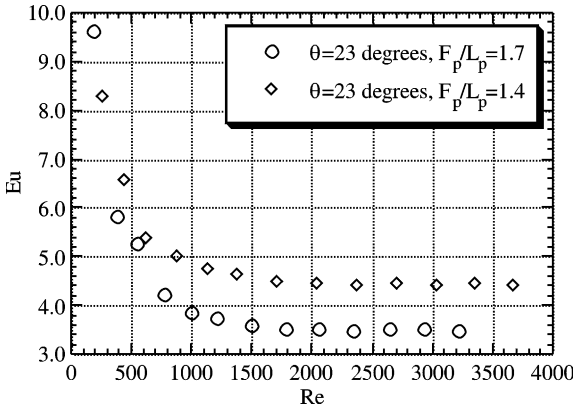

Fig. 6. Plot showing the effect of the fin- to louver-pitch ratio on pressure drop through a louvered-fin array.

The flow visualization results shown in Fig. 7 further illustrate the effect of Reynolds number on flow through louver arrays (All white horizontal and vertical lines in the flow visualization photographs are supports that do not extend into the flow and can be ignored.). A comparison of Fig. 7a and b shows that as the Reynolds number increases, in this case from 260 to 670, the flow efficiency increases. Additional increases in Reynolds number, while not affecting the flow efficiency, cause the flow to become unsteady. In Fig. 7c, where $Re = 1130$, the flow in the downstream half of the array has become unsteady.

The Reynolds number at which a given row of louvers begins to shed vortices from their leading edges is

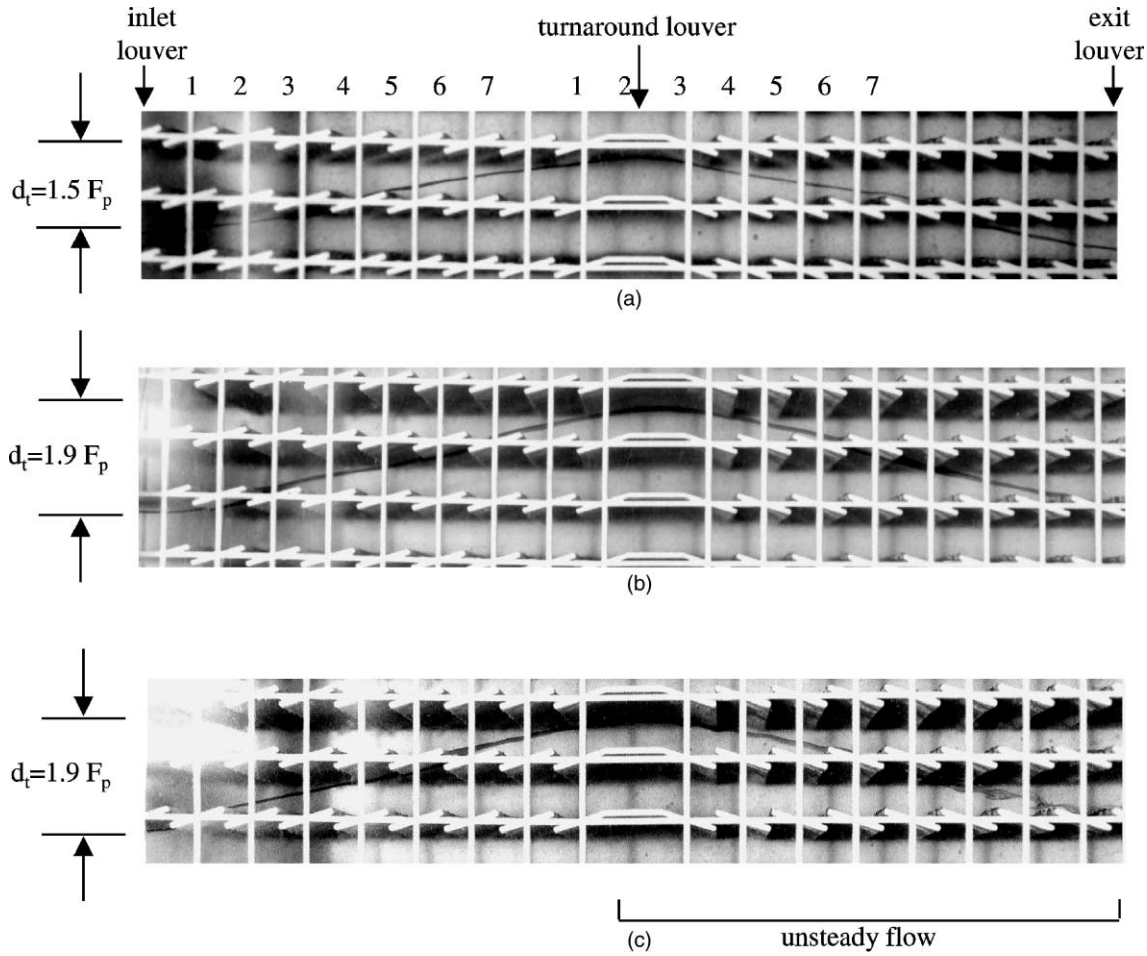

Fig. 7. Flow through an array with $\theta = 18°$ and $F_p/L_p = 1.09$ at (a) $Re = 260$, (b) $Re = 670$ and (c) $Re = 1130$.

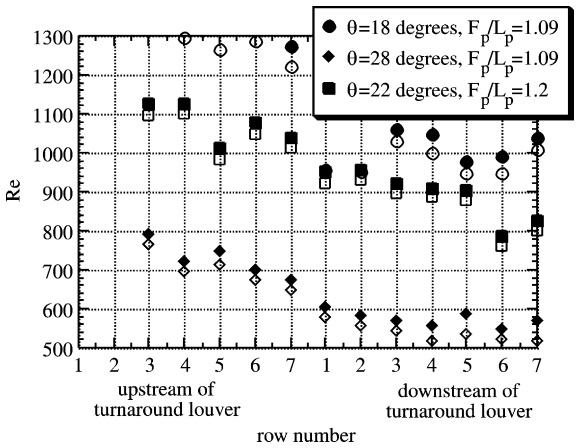

Fig. 8. The Reynolds number at which a given row of louvers in an array begins to shed vortices from their leading edges. Below that Reynolds number the flow is steady and laminar at that location within the array. The clear symbols indicate the Reynolds number at which very weak, small vortices are noted. The dark symbols indicate the Reynolds number at which larger vortices are clearly shed (refer to Fig. 7 for louver numbering).

shown in Fig. 8 (see Fig. 7 for louver numbering). At low Reynolds numbers the flow is steady and laminar. Then as the Reynolds number is increased, small-scale periodic transverse velocity fluctuations generated upstream propagate downstream, and louvers downstream of the turnaround louver start to shed small spanwise vortices. Previous studies [29,36] showed the onset of vortex shedding in the offset-strip geometry to depend on Reynolds number and position in the array. In that geometry, like the louvered-fin geometry, the flow is steady and laminar at low Reynolds numbers. As the Reynolds number is increased, the furthest row of fins downstream begins to shed vortices, and as the Reynolds number is increased further, the onset of vortex shedding moves upstream. In the offset-strip fin geometry, the vortices are clear and distinct, and the Reynolds number of onset is fairly easy to determine. For louvered fins, the flow becomes unsteady gradually; the vortices are smaller, and it is difficult to determine an exact Reynolds number at which a given row of louvers begins to shed vortices. Thus, two Reynolds numbers are given for most positions in Fig. 8—the Reynolds number at which small, weak vortices are first noted, and the Reynolds number at which larger vortices are clearly present. The uncertainty of these values is roughly 11%. This estimate includes the uncertainty of the Reynolds number (10%) and the 5% scatter in the data acquired for a given row. These findings are in agreement with trends reported in the numerical study of Tafti and Zhang [20], and although unsteadiness onset is experimentally observed at somewhat higher Reynolds numbers than numerical predictions (see [18]), the differences are probably due to the limitations of a localized dye streak—in contrast to full field information from numerical studies.

Flow through a louvered-fin array is similar to flow through an offset-strip array; however, in the louvered-fin array the distance along a streamline from one louver to the next is longer relative to the louver size than in the offset-strip array (note the flow visualization in Fig. 7). Thus, small-scale periodic transverse velocity fluctuations generated by upstream louvers are more likely to die out in the louvered-fin geometry before reaching downstream louvers. This geometrical feature explains why there is a larger Reynolds number range between the onset of unsteadiness in fin wakes and the shedding of discrete vortices from louvers. As the louver angle increases and the flow efficiency with it, the flow distance between louvers decreases, and the array begins to shed vortices at a lower Reynolds number (cf. $\theta = 28$–18° in Fig. 8).

The data in Fig. 8 show that downstream of the turnaround, the onset of vortex shedding has little spatial dependence within the array. In contrast to the offset-strip array, a streakline passing by a louver in the downstream half of the louver array did not necessarily pass by every upstream louver on that fin. Thus, the number of upstream interruptions, and thus the extent of perturbation, depends on the flow efficiency, which in turn depends on the geometry and Reynolds number. Whereas the onset of shedding in an offset-strip array depends strongly in location in the array, this dependence is small in the louver array. This behavior is a direct result of the flow-directing properties of the louvers. Louvers in the first two rows of the array (upstream of the turnaround louver) were not noted to shed vortices from their leading edges in the Reynolds number range of operation. The flow approaching the first two rows was not in the wake of any upstream louvers, and thus the flow was steady and laminar. However, louvers in row 2 were noted to shed vortices from their trailing edges. This finding is consistent with observations of flow in offset-strip arrays.

Fig. 9 shows the unsteady flow features more closely. These photographs are of flow through a geometry with $\theta = 28^\circ$ and $F_p/L_p = 1.09$, but similar flow structures were noted in each of the geometries tested. At a Reynolds number of 660 (Fig. 9a), small transverse vortices are shed periodically from the leading edges of louvers downstream of the turnaround. The flow upstream of the turnaround is steady and laminar except for small vortices being shed from row 7 (not shown in the figure). At $Re = 730$, shown in Fig. 9b, discrete vortices can be seen in the flow passing by rows 5–7 (upstream of the turnaround). Downstream of the turnaround the flow is characterized by extensive mixing. Fig. 9c shows small vortices being shed from the leading edge of row 3 (upstream) at $Re = 920$. The flow downstream (not

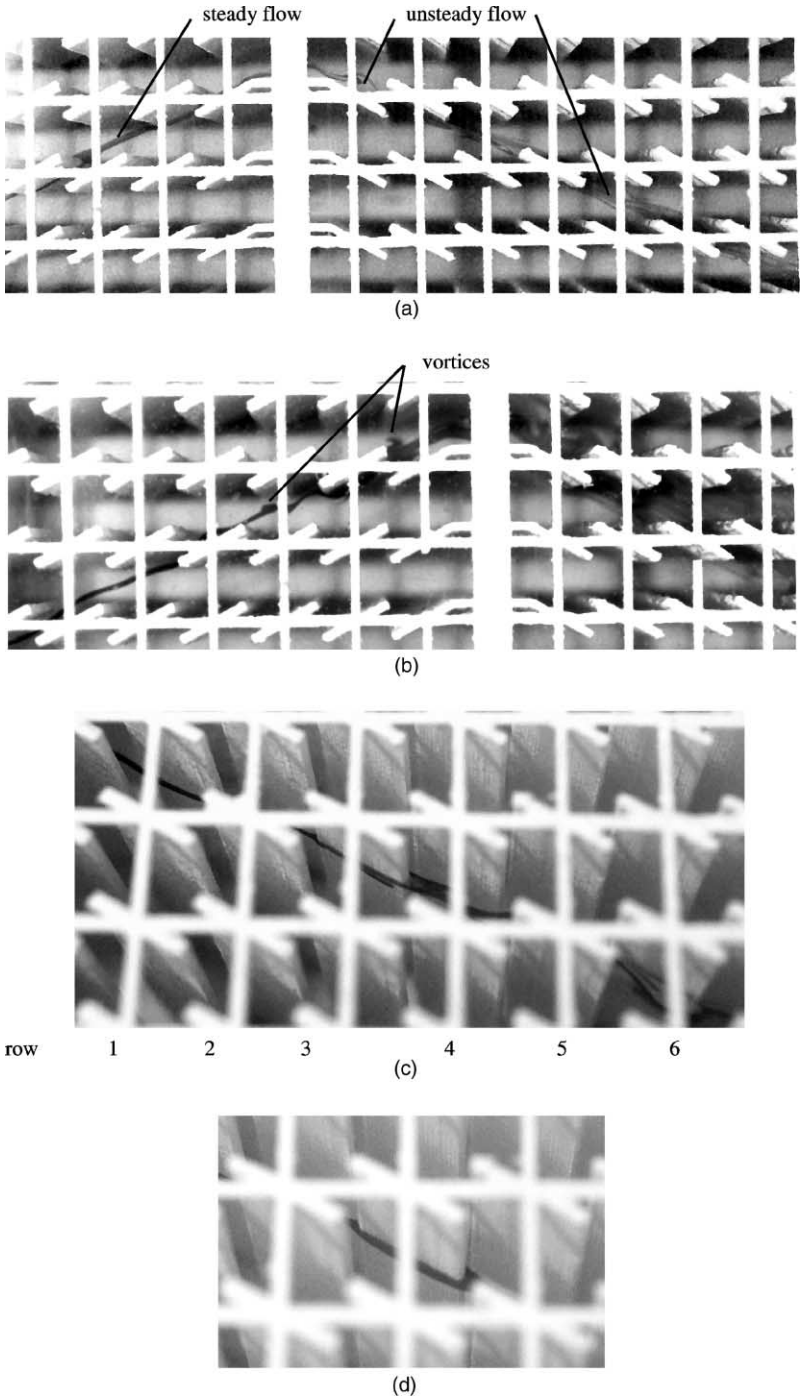

Fig. 9. Flow through an array with $\theta = 28^\circ$ and $F_p/L_p = 1.09$. (a) At $Re = 660$, small vortices are being shed from the last row upstream of the turnaround louver, and larger vortices are being shed downstream. Further upstream the flow is steady. (b) By $Re = 730$, several rows of louvers upstream of the turnaround are also shedding vortices. The flow downstream of the turnaround louver is characterized by extensive mixing. (c) At $Re = 920$, vortices can be seen shedding from the third row of louvers (upstream of the turnaround louver). (d) At $Re = 270$, the flow is steady.

shown in the photograph) shows more mixing. Fig. 9c can be contrasted with Fig. 9d which shows steady flow past a louver in the same geometry at $Re = 270$.

3.2. Mass transfer results

Louver-by-louver mass transfer results are presented in Fig. 10 for three different arrays. Row 1, upstream of the turnaround louver, follows the inlet louver, and the exit louver follows row 7, downstream of the turnaround louver. The mass (and hence heat) transfer coefficients are approximately constant throughout the array except near the turnaround louver. As discussed earlier, thermal wakes are mostly recovered as the flow passes from louver to louver. Therefore, downstream fin heat transfer coefficients are not discernibly affected by upstream louvers.

The turnaround louver shows a significantly lower mass transfer coefficient than the other louvers. Note that the length scale used for the Sherwood number of the turnaround louver is the same as the length scale used for the other louvers ($L_p = 11.9$ mm). The average boundary-layer thickness on the turnaround louver is larger than on the other louvers because the turnaround louver is three times as long. Similar to the results of Aoki et al. [22] data for the $\theta = 18°$ geometry as well as the data for the $\theta = 28°$ and 22° for $Re < 600$ show a "recovery length" consisting of one to three rows of louvers downstream of the turnaround louver, depending on the geometry and Reynolds number. In this recovery length, the mass transfer coefficient increases from the mass transfer coefficient of the turnaround louver to the value of the rows upstream. At the downstream edge of the turnaround louver, the velocity boundary layer is thick. This thick boundary layer, which passes through the louver gap between the turnaround louver and the adjacent louver downstream, decreases the flow rate through this louver gap, and thus the local flow efficiency is decreased just downstream of the turnaround. This effect is shown by the asymmetry of the streamline in Fig. 11. Hence, the velocity must be lower, and the mass transfer coefficient is decreased just downstream of the turnaround. This decrease is larger for small louver angles and low Reynolds numbers. At low Reynolds numbers the boundary layers are thicker and occupy a larger percentage of the louver gap than at higher Reynolds numbers. In the same way, the louver gap is smaller for lower louver angles, so at a particular Reynolds number the boundary layers take up a larger percentage of the louver gap.

Fig. 12 shows the array-averaged mass transfer results for three different geometries. As expected, an increase in the louver angle increases mass transfer. An increase in the louver angle results in a longer flow path and a higher flow efficiency. With a larger flow efficiency, a larger percentage of this longer flow path is spent between the louvers rather than in the duct between fins. The heat transfer coefficient for developing flow in a narrow duct (such as between louvers) is higher than that for a wider duct (see the results of Huang and Fan [35]). Here, increasing the louver angle by 10° increases mass transfer by approximately 25–35% (however, the pressure drop increases by approximately 100%). The earlier onset of unsteady flow for the geometry with $\theta = 28°$ does not cause a discernible increase in mass transfer. The difference in Sherwood numbers between the $\theta = 28°$ geometry and the $\theta = 18°$ geometry is approximately constant throughout the Reynolds number range. The difference does not increase for those Reynolds numbers where the flow in the $\theta = 28°$ geometry is unsteady whereas the flow in the $\theta = 18°$ geometry is steady. While an increase in louver angle increases the mass-transfer coefficient, an increase in fin pitch decreases the mass-transfer coefficient. Although the current study does not provide enough data to prove that effect, Chang and Wang [5] show a weak dependence of Colburn j factor on F_p/L_p (-0.14 power).

Previous studies of offset-strip fins show a distinct increase in heat transfer when fins began to shed vortices [29]. The onset of vortex shedding is clear and fairly abrupt, and as a louver begins to shed vortices from its leading edge, its heat (mass) transfer increases significantly in the offset-strip array. However, as discussed earlier, the onset of vortex shedding in the louvered-fin geometry is much more gradual. Unsteadiness increases over a Reynolds number range, and the resulting vortices are small. Thus, it is difficult to determine the effect of vortex shedding on heat transfer in this geometry. For the geometry used in Fig. 10b—the geometry that showed the strongest vortex shedding—the rows downstream of the turnaround louver shed vortices at a Reynolds number of 610 while the rows upstream were not shedding vortices. At a Reynolds number of 710, many of the upstream rows were also shedding vortices. Therefore, if vortex shedding had a significant effect on heat transfer, the Sherwood numbers of the upstream rows should have increased significantly from a Reynolds number of 610–710. However, Fig. 10b shows the Sherwood numbers to be identical within the 5% uncertainty of the measurements. The mass-transfer behavior appears much the same throughout the Reynolds number range even though at low Reynolds numbers the flow was steady while at high Reynolds numbers it was definitely unsteady. The percentage difference between the array-averaged Sherwood numbers for the $\theta = 18°$ and 28° geometries presented in Fig. 12 remains approximately constant throughout the Reynolds number range even though flow through the $\theta = 28°$ geometry became unsteady at a much lower Reynolds number. If vortex shedding increased mass transfer significantly, this difference would have increased for the $Re = 610$ and 990 cases when the flow in the $\theta = 28°$ geometry exhibited periodic vortex shedding but the flow through

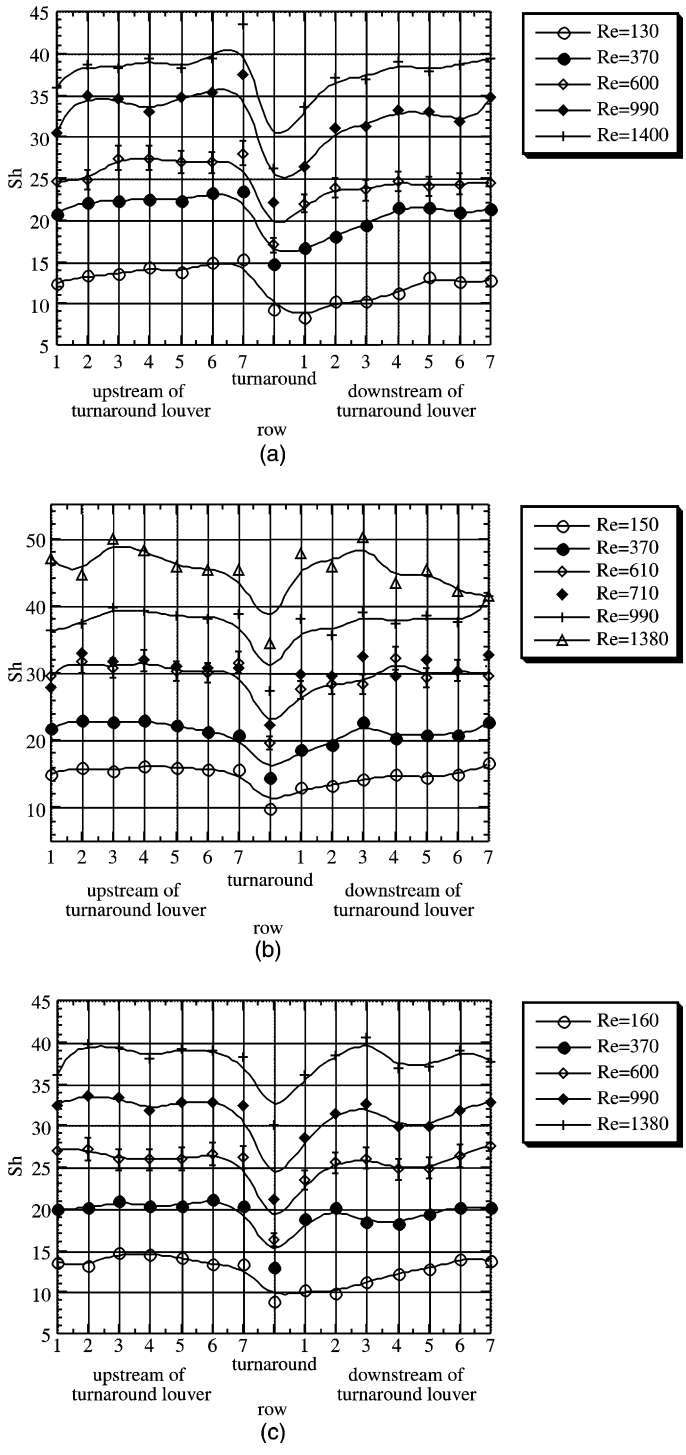

Fig. 10. Sherwood numbers shown on a louver-by-louver basis for three different geometries over a Reynolds number range of 75–1400. Row 1, upstream of the turnaround louver, follows the inlet louver, and the exit louver follows row 7, downstream of the turnaround louver. (a) $\theta = 18°$, $F_p/L_p = 1.09$, (b) $\theta = 28°$, $F_p/L_p = 1.09$ and (c) $\theta = 22°$, $F_p/L_p = 1.2$. The lines are simple smooth curve fits to the data.

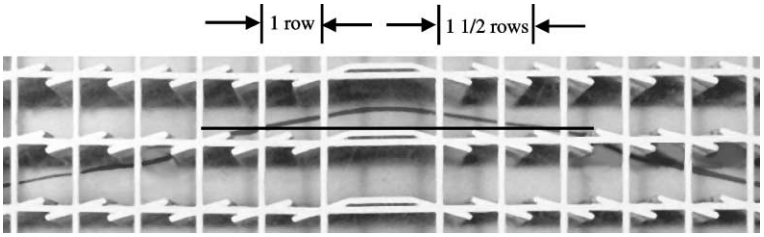

Fig. 11. Here at $Re = 260$ for $\theta = 18°$ and $F_p/L_p = 1.09$, the flow is not symmetric around the turnaround louver. An additional streamline (which is not shown) passes over the turnaround louver. The local reduction in flow efficiency downstream of the turnaround louver causes the "recovery zone" shown in Fig. 10.

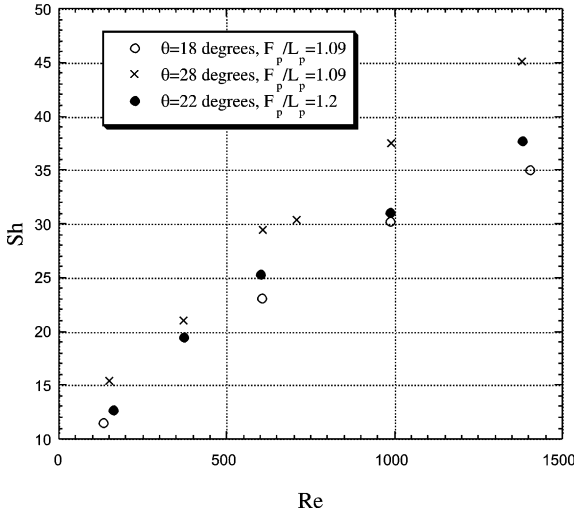

Fig. 12. Array-averaged Sherwood numbers plotted versus Reynolds number for three different arrays.

the $\theta = 18°$ geometry was steady and laminar. In addition, at $Re = 610$ for the geometry used in Fig. 10b and $Re = 990$ for Fig. 10c, the downstream louvers were shedding vortices while most of the upstream louvers were not. Yet the heat transfer coefficients of the downstream louvers were the same as the heat transfer coefficients of the upstream louvers. For the highest Reynolds number cases ($Re = 1400$ in Fig. 10a, $Re = 1380$ and 990 for Fig. 10b, and $Re = 1380$ for Fig. 10c), there is no discernible increase in mass transfer from row 2 (where vortices were not shed from the louver leading edges) to row 3 (where vortices were shed from the louver leading edges). Therefore, it is concluded that vortex shedding has a very small effect on mass (heat) transfer under these conditions.

4. Summary and conclusions

In this paper, flow efficiency, pressure drop, and heat transfer behavior in louvered-fin arrays have been discussed. Louver-by-louver mass-transfer results (which are analogous to heat transfer results) have been presented for three arrays over a Reynolds number range of 130–1400. Mass (heat) transfer coefficients were noted to be fairly constant though the array except for low mass-transfer coefficients on the turnaround louver and in a recovery zone just downstream of the turnaround louver in some cases. The low mass-transfer coefficients were related to low velocities between the louvers caused by thick velocity boundary layers on the turnaround, which resulted in the deflection of streamlines into the inter-fin duct. Vortex shedding caused only very small increases in mass transfer (within the 5% experimental uncertainty.).

The results presented in this paper have practical implications. Designers might consider methods for minimizing the heat transfer penalty associated with the recovery zone and the turnaround louver. It may be possible to increase the size of the louver gap just downstream of the turnaround by increasing the louver angle of the first row or two downstream of the turnaround to minimize the recovery zone. It is desirable to keep the displacement thickness on the turnaround louver to less than approximately 30% of the louver gap. Decreasing the length of the turnaround louver will also decrease the size of the recovery zone and increase average heat transfer on the turnaround louver. Short inlet and exit louvers are also desirable. However, even for a low louver angle of 18°, the decrease in average heat transfer due to the recovery zone reached a maximum of 7% at a Reynolds number of 130. A large increase in manufacturing cost may not be justified by the limited benefit of reducing or removing the turnaround (which is currently used to ease manufacturing). It should be noted that removing the turnaround in small heat exchangers with less than 100 fins could have an adverse impact on thermal performance through increased wall effects on the array (see [15]).

Finally, in contrast to the offset-strip fin, vortex shedding in the louvered-fin geometry causes only small increases in heat transfer (and pressure drop) over the Reynolds number range of interest. Designers need not

strive to operate the louvered fin in the transitional regime where fins shed vortices. Furthermore, since vortex shedding has much less impact on the thermal–hydraulic performance of louvered-fin arrays, steady-state computational models of louver arrays may be expected provide accurate predictions of flow and heat transfer over a wider Reynolds number range than in other interrupted-fin arrays.

Acknowledgements

The authors gratefully acknowledge the financial support of the ACRC, an industry–university cooperative research center, founded by the NSF in 1989.

References

[1] C.J. Davenport, Heat transfer and flow friction characteristics of louvered heat exchanger surfaces, in: J. Taborek, G.F. Hewitt, N. Afgan (Eds.), Heat Exchangers: Theory and Practice, Hemisphere, Washington, DC, 1983, pp. 397–412.

[2] C.J. Davenport, Correlations for heat transfer and flow friction characteristics of louvered fin, AIChE Symp. Ser. 225 (79) (1983) 19–27.

[3] A. Achaichia, T.A. Cowell, Heat transfer and pressure drop characteristics of flat tube and louvered plate fin surfaces, Exp. Therm. Fluid Sci. 1 (1988) 147–157.

[4] Y.-J. Chang, C.-C. Wang, Air side performance of brazed aluminum heat exchangers, J. Enhanc. Heat Transfer 3 (1996) 15–28.

[5] Y.-J. Chang, C.-C. Wang, A generalized heat transfer correlation for louver fin geometry, Int. J. Heat Mass Transfer 40 (1997) 533–544.

[6] A. Achaichia, T.A. Cowell, A finite difference analysis of fully developed periodic laminar flow in inclined louver arrays, in: Proceedings of the 2nd UK National Heat Transfer Conference, vol. 1, Glasgow, 1988, pp. 883–898.

[7] M. Hiramatsu, T. Ishimaru, K. Matsuzaki, Research on fins for air conditioning heat exchangers, JSME Int. J., Ser. II 33 (4) (1990) 749–756.

[8] K. Suga, H. Aoki, T. Shinagawa, Numerical analysis on two-dimensional flow and heat transfer of louvered fins using overlaid grids, JSME Int. J., Ser. II 33 (1990) 122–127.

[9] K. Suga, H. Aoki, Numerical study on heat transfer and pressure drop on multilouvered fins, ASME/JSME Thermal Engineering Proceedings, vol. 4, ASME, New York, NY, 1991, pp. 361–368.

[10] A. Sahnoun, R.L. Webb, Prediction of heat transfer and friction for the louver fin geometry, J. Heat Transfer 114 (1992) 893–900.

[11] E.R. Dillen, R.L. Webb, Rationally based heat transfer and friction correlations for the louver fin geometry, SAE Paper 950504, Society of Automotive Engineers, Detroit, MI, 1994.

[12] R.L. Webb, P. Trauger, Flow structure in the louvered fin heat exchanger geometry, Exp. Therm. Fluid Sci. 4 (1991) 205–217.

[13] K. Bellows, Flow visualization of louvered-fin heat exchangers, ACRC Technical Report 124, University of Illinois, Urbana, IL, 1997.

[14] T.A. Cowell, M.R. Heikal, A. Achaichia, Flow and heat transfer in compact louvered fin surfaces, Exp. Therm. Fluid Sci. 10 (1995) 192–199.

[15] N.C. DeJong, Flow, heat transfer, and pressure drop interactions in louvered-fin arrays, Ph.D. thesis, University of Illinois, Urbana, IL, 1999.

[16] R.K. Shah, M.R. Heikal, B. Thonon, Advances in numerical analysis of fluid flow, heat transfer and flow friction characteristics of compact heat exchanger surfaces, in: G. de Vahl Davis, E. Leonardi (Eds.), CHT97: Advances in Computational Heat Transfer, Begall House, New York, 1998, pp. 68–87.

[17] R.K. Shah, M.R. Heikal, B. Thonon, P. Tochon, Progress in numerical analysis of compact heat exchanger surfaces, in: J.P. Hartnett (Ed.), Advances in Heat Transfer, vol. 34, Academic Press, New York, NY, 2000, pp. 363–443.

[18] D.K. Tafti, G. Wang, W. Lin, Flow transition in a multilouvered fin array, Int. J. Heat Mass Transfer 43 (2000) 901–919.

[19] X. Zhang, D.K. Tafti, Classification and effects of thermal wakes on heat transfer in multilouvered fins, Int. J. Heat Mass Transfer 44 (2001) 2461–2473.

[20] D.K. Tafti, X. Zhang, Geometry effects on flow transition in multilouvered fins—onset, propagation, and characteristic frequencies, Int. J. Heat Mass Transfer 44 (2001) 4195–4210.

[21] M.E. Springer, K.A. Thole, Entry region of louvered fin heat exchangers, Exp. Therm. Fluid Sci. 19 (1999) 223–232.

[22] H. Aoki, T. Shinagawa, K. Suga, An experimental study of the local heat transfer characteristics in automotive louvered fins, Exp. Therm. Fluid Sci. 2 (1989) 293–300.

[23] L.W. Zhang, A numerical study of flow and heat transfer in compact heat exchangers, Ph.D. thesis, University of Illinois, Urbana, IL, 1996.

[24] M.E. Springer, K.A. Thole, Experimental design of flow-field studies of louvered fins, Exp. Therm. Fluid Sci. 18 (1998) 258–269.

[25] A.A. Antoniou, M.R. Heikal, T.A. Cowell, Measurements of local velocity and turbulence levels in arrays of louvered plate fins, in: G. Hetsroni (Ed.), Heat Transfer 1990, vol. 4, Hemisphere Publishing, Washington, DC, 1990, pp. 105–110.

[26] R.S. Mullisen, R.I. Loehrke, A study of the flow mechanisms responsible for heat transfer enhancement in interrupted-plate heat exchangers, J. Heat Transfer 108 (1986) 377–385.

[27] G. Xi, S. Futagami, Y. Hagiwara, K. Suzuki, Flow and heat transfer characteristics of offset-fin array in the middle Reynolds number range, ASME/JSME Thermal Engineering Proceedings, vol. 3, ASME, New York, NY, 1991, pp. 151–156.

[28] L.W. Zhang, S. Balachandar, D.K. Tafti, F.M. Najjar, Heat transfer enhancement mechanisms in inline and staggered parallel-plate fin heat exchangers, Int. J. Heat Mass Transfer 40 (1997) 2307–2325.

[29] N.C. DeJong, A.M. Jacobi, An experimental study of flow and heat transfer in parallel-plate arrays: local, row-by-row and surface average behavior, Int. J. Heat Mass Transfer 40 (1997) 1365–1378.

[30] R.J. Goldstein, H.H. Cho, A review of mass transfer measurements using the naphthalene sublimation technique, Exp. Therm. Fluid Sci. 10 (1995) 416–434.

[31] P.R. Souza Mendes, A review of mass transfer measurements using the naphthalene sublimation technique, Exp. Therm. Fluid Sci. 4 (1991) 510–523.

[32] N.C. DeJong, L.W. Zhang, A.M. Jacobi, S. Balachandar, D.K. Tafti, A complementary experimental and numerical study of the flow and heat transfer in offset strip-fin heat exchangers, J. Heat Transfer 120 (1998) 690–698.

[33] E.M. Sparrow, A. Hajiloo, Measurements of heat transfer and pressure drop for an array of staggered plates aligned parallel to an air flow, J. Heat Transfer 102 (1980) 426–432.

[34] S.J. Kline, F.A. McClintock, Describing uncertainties in single sample experiments, Mech. Eng. 75 (1953) 3–8.

[35] R.K. Shah, M.S. Bhatti, Laminar convective heat transfer in ducts, in: S. Kakaç, R.K. Shah, W. Aung (Eds.), Handbook of Single-Phase Convective Heat Transfer, John Wiley and Sons, New York, NY, 1987.

[36] S. Mochizuki, Y. Yagi, Characteristics of vortex shedding in plate arrays, in: W. Merzkirch (Ed.), Flow Visualization, Hemisphere Publishing, Washington, DC, 1982, pp. 99–103.